J|A|C|S
ARTICLES
Published on Web 03/24/2007

Carbohydrate-Coated Supramolecular Structures: Transformation of Nanofibers into Spherical Micelles Triggered by Guest Encapsulation

Ja-Hyoung Ryu, Eunji Lee, Yong-beom Lim, and Myongsoo Lee*

Contribution from the Center for Supramolecular Nano-Assembly and Department of Chemistry, Yonsei University, Seoul 120-749, Korea

Received January 9, 2007; E-mail: mslee@yonsei.ac.kr

Abstract: Triblock rigid-flexible dendritic block molecules consisting of a rigid aromatic segment as a stem segment, carbohydrate-branched dendrons as a flexible head, and a hydrophobic alkyl chain were synthesized and characterized. The carbohydrate conjugate molecule based on a methyl group as a hydrophobic tail, in the solid state, self-assembles into a 1D nanostructure, whereas the molecule based on a longer hydrophobic tail self-assembles into 2D nanosheets, as confirmed by X-ray scatterings. In aqueous solution, however, both molecules were observed to self-assemble into carbohydrate-coated cylindrical aggregates with a uniform diameter, as confirmed by dynamic light scatterings and transmission electron microscopic (TEM) investigations. Notably, these cylindrical objects reversibly transformed into spherical objects on addition of guest molecules. Investigation of the interactions of the carbohydrate-coated nanostructures with *E. coli* cells showed that both nano-objects could immobilize bacterial cells, while the degrees of immobilization were significantly dependent on the shape of nanostructure. These results demonstrated that the supramolecular materials that are responsive to external stimuli can provide novel opportunities to control many biological activities.

Introduction

Controlled self-assembly of incompatible molecular components can lead to a variety of nanostructures including spherical micelles, vesicles, nanofibers, toroids, and tubes.[1] The construction of supramolecular architectures by the self-assembly of designed molecules is thus a subject of great current interest and a challenging topic of interdisciplinary research in chemistry, biology, and materials science.[2] In particular, self-organization of carbohydrate conjugate molecules can endow nanostructures with biological functions as multivalent ligands.[3,4] Although many different designs of multivalent ligands such as glycoprotiens,[5] linear polymers,[6] and dendrimers[7] have been reported, the self-assembly that plays a key role in living systems provides a powerful approach toward the fabrication of complex nanoarchitectures. Precise control of molecular arrangements of self-assembling molecules at the supramolecular level is essential to get well-defined nanoscopic architectures as well as desired biological functions.[8] Introducing a rigid segment into a self-assembling system has been reported to enhance aggregation stability.[9] In addition to stability, another important issue regarding the preparation of these self-assembling systems is their capability to respond to external stimuli such as pH, temperature, and interaction with guest molecules and to interact with biological receptors.[10−12] To obtain precisely controlled

(1) (a) Jain, S.; Bates, F. S. *Science* **2003**, *300*, 460−464. (b) Discher, D. E.; Eisenberg, A. *Science* **2002**, *297*, 967−973. (c) Yang, W.-Y.; Ahn, J.-H.; Yoo, Y.-S.; Oh, N.-K.; Lee, M. *Nat. Mater.* **2005**, *5*, 399−402. (d) Shimizu, T.; Masuda, M.; Minamikawa, H. *Chem. Rev.* **2005**, *105*, 1401−1444. (e) Kim, J.-K.; Lee, E.; Huang, Z.; Lee, M. *J. Am. Chem. Soc.* **2006**, *128*, 14022−14023. (f) Ryu, J.-H.; Cho, B.-K.; Lee, M. *Bull. Korean Chem. Soc.* **2006**, *27*, 1270−1282. (g) Kawasaki, T.; Tokuhiro, M.; Kimizuka, N.; Kunitake, T. *J. Am. Chem. Soc.* **2001**, *123*, 6792−6800.

(2) (a) Lehn, J. M. *Supramolecular Chemistry, Concepts and Perspectives*; VCH: Weinheim, Germany, 1995. (b) Hoeben, F. J. M.; Jonkheijm, P.; Meijer, E. W.; Schenning, A. P. H. J. *Chem. Rev.* **2005**, *105*, 1491−1546. (c) Cornelissen, J. J. L. M.; Rowan, A. E.; Nolte, R. J. M.; Sommerdijk, N. A. J. M. *Chem. Rev.* **2001**, *101*, 4039−4070. (d) Ajayaghosh, A.; Vijayakumar, C.; Varghese, R.; George, S. J. *Angew. Chem., Int. Ed.* **2006**, *45*, 456−460. (e) Motoyanagi, J.; Fukushima, T.; Ishii, N.; Aida, T. *J. Am. Chem. Soc.* **2006**, *128*, 4220−4221. (f) Zhang, S. G. *Nat. Biotechol.* **2003**, *21*, 1171−1178. (g) Lee, M.; Cho, B.-K.; Zin, W.-C. *Chem. Rev.* **2001**, *101*, 3869−3892. (h) Chen, B.; Baumeister, U.; Pelzl, G.; Das, M. K.; Zeng, X.; Ungar, G.; Tschierske, C. *J. Am. Chem. Soc.* **2005**, *127*, 16578−16591.

(3) (a) Thoma, G.; Katopodis, A. G.; Voelcker, N.; Duthaler, R. O.; Streiff, M. B. *Angew. Chem., Int. Ed.* **2002**, *41*, 3195−3198. (b) Aoyama, Y.; Kanamori, T.; Nakai, T.; Sasaki, T.; Horiuchi, S.; Sando, S.; Niidome, T. *J. Am. Chem. Soc.* **2003**, *125*, 3455−3457.

(4) (a) de la Fuente, J. M.; Barrientos, A. G.; Rojas, T. C.; Rojo, J.; Cañada, J.; Fernández, A.; Penadés, S. *Angew. Chem., Int. Ed.* **2001**, *40*, 2258−2261. (b) Lin, C.-C.; Yeh, Y.-C.; Yang, C.-Y.; Chen, C.-L.; Chen, G.-F.; Chen, C.-C.; Wu, Y.-C. *J. Am. Chem. Soc.* **2002**, *124*, 3508−3509. (c) Osaki, F.; Kanamori, T.; Sando, S.; Sera, T.; Aoyama, Y. *J. Am. Chem. Soc.* **2004**, *126*, 6520−6521.

(5) Bertozzi, C. R.; Kiessling, L. L. *Science* **2001**, *291*, 2357−2364.

(6) (a) Disney, M. D.; Zheng, J.; Swager, T. M.; Seeberger, P. H. *J. Am. Chem. Soc.* **2004**, *126*, 13343−13346. (b) Gestwicki, J. E.; Kiessling, L. L. *Nature* **2002**, *415*, 81−84. (c) Sasaki, K.; Nishida, Y.; Tsurumi, T.; Uzawa, H.; Kondo, H.; Kobayashi, K. *Angew. Chem., Int. Ed.* **2002**, *41*, 4463−4467. (d) Cario, C. W.; Gestwicki, J. E.; Kanai, M.; Kiessling, L. L. *J. Am. Chem. Soc.* **2002**, *124*, 1615−1619.

(7) (a) Wolfenden, E. K.; Cloninger, M. J. *J. Am. Chem. Soc.* **2005**, *127*, 12168−12169. (b) Roy, R.; Kim, J. M. *Angew. Chem., Int. Ed.* **1998**, *38*, 369−372. (c) Woller, E. K.; Walter, E. D.; Morgan, J. R.; Singel, D. J.; Cloninger, M. J. *J. Am. Chem. Soc.* **2003**, *125*, 8820−8826.

(8) (a) Wong, G. C. L.; Tang, J. X.; Lin, A.; Li, Y.; Janmey, P. A.; Safinya, C. R. *Science* **2000**, *288*, 2035−2039. (b) Elemans, J. A. A. W.; Rowan, A. E.; Nolte, R. J. M. *J. Mater. Chem.* **2003**, *13*, 2661−2670. (c) Hartgerink, J. D.; Beniash, E.; Stupp, S. I. *Science* **2001**, *294*, 1684−1687. (d) Percec, V.; Dulcey, A. E.; Balagurusamy, V. S. K.; Miura, Y.; Smidrkal, J.; Peterca, M.; Nummelin, S.; Edlund, U.; Hudson, S. D.; Heiney, P. A.; Duan, H.; Magonov, S. N.; Vinogradov, S. A. *Nature* **2004**, *430*, 764−768.

10.1021/ja070173p CCC: $37.00

Scheme 1. Synthesis of the Carbohydrate Conjugate Aromatic Amphiphiles

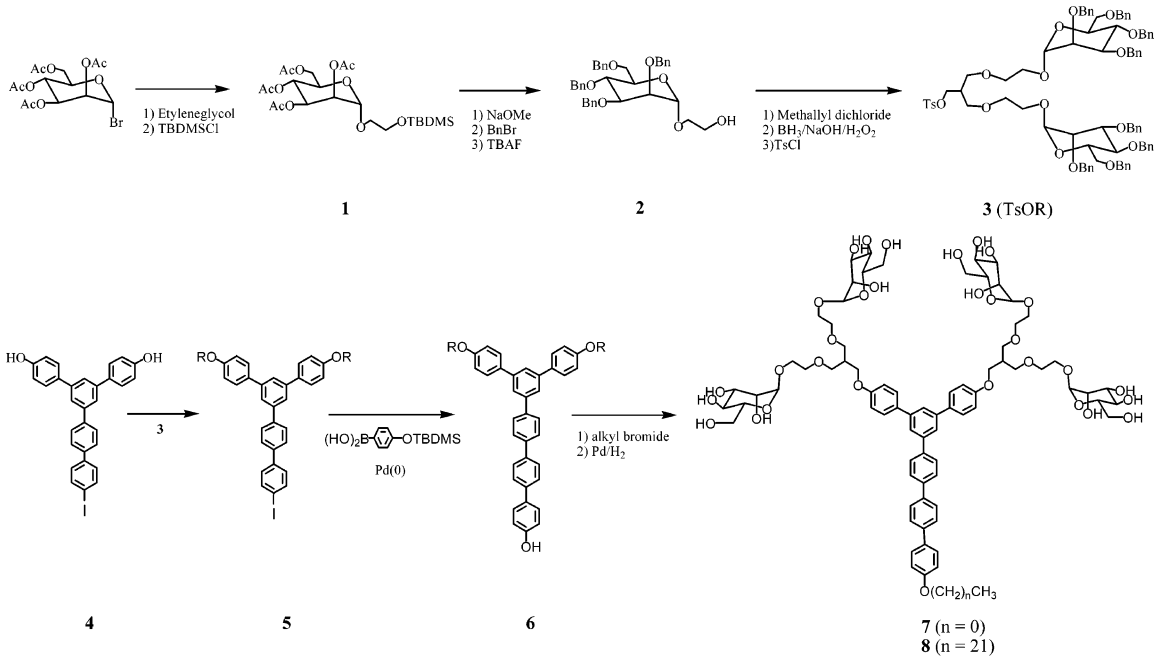

and well-defined aggregates that are able to respond to external stimuli such as interaction with guest molecules, however, the more elaborate design of corresponding building blocks is required, because the information determining their specific assembly should be encoded in their molecular architecture. Accordingly, we synthesized carbohydrate conjugate aromatic molecules that can endow aggregates with enhanced stability, external stimuli responsive character, and biological functions. We present herein the formation of carbohydrate-coated nanofibers from the self-assembly of carbohydrate conjugate aromatic amphiphiles in aqueous solution and reversible switching between fibers and spheres triggered by addition of guest molecules. Notably, the specific multivalent interactions of carbohydrate residues in the nanostructures with cognate binding proteins in the pili of *E. coli* resulted in the shape-dependent motility inhibition.

Results and Discussion

Synthesis. The triblock rigid aromatic-flexible dendritic block molecules consisting of a hydrophobic alkyl chain, a rigid aromatic segment, and flexible carbohydrate conjugate dendrons were obtained in a multiple synthesis from commercially available starting materials (Scheme 1).

The design of a dendritic flexible chain was focused on the construction of a carbohydrate conjugate segment that is soluble in water and can have selectivity in bacterial cells. Mannose containing dendron (**3**) was synthesized by glycosylation of peracetylated bromo-D-mannose with ethylene glycol and change of deprotection group from the acetyl to benzyl group, which is more stable in basic conditions, and the subsequent convergent route of oligoether dendron using etherification chemistry. The aromatic core (**4**) prepared according to the procedures described previously[13] and then the subsequent etherification with tosylated mannose conjugate dendron yielded **5**, showing sufficient solubility for further couplings of rigid conjugated building blocks in the reaction medium. **6** was prepared from the Suzuki coupling reaction with **5** and 4-hydroxy phenyl boronic acid in the presence of Pd(0) catalysis. The final carbohydrate conjugate molecules were synthesized by etherification of **6** and alkyl halide and subsequent deprotection of the benzyl protecting groups with Pd charcoal under H_2 atmosphere. The resulting carbohydrate conjugate aromatic amphiphiles (**7** and **8**) were characterized by ^{1}H and ^{13}C NMR spectroscopy, elemental analysis, and MALDI-TOF mass spectroscopy and were shown to be in full agreement with the structures presented. As confirmed by ^{1}H NMR spectroscopy, the ratio of the aromatic protons of the rod block to the alkyl protons is consistent with the ratio calculated. As shown in Figure 1, the MALDI-TOF mass spectra of the carbohydrate conjugate aromatic molecules exhibit three signals that can be assigned as the molecular ions, together with the Na^+ and K^+ labeled molecular ions. The mass corresponding to a representative peak in the spectrum is matched with the calculated molecular weight of each of the carbohydrate conjugate aromatic molecules.

Solid-State Structure. The self-assembling behavior of the carbohydrate conjugate aromatic molecules in the bulk was investigated by means of thermal optical polarized microscopy

(9) (a) Yoo, Y.-S.; Choi, J.-H.; Song, J.-H.; Oh, N.-K.; Zin, W.-C.; Park, S.; Chang, T.; Lee, M. *J. Am. Chem. Soc.* **2004**, *126*, 6294−6300. (b) Discher, B. M.; Won, Y. Y.; Ege, D. S.; Lee, J. C. M.; Bates, F. S.; Discher, D. E.; Hammer, D. A. *Science* **1999**, *284*, 1143−1146. (c) Kukula, H.; Schlaad, H.; Antoniett, M.; Föster, S. *J. Am. Chem. Soc.* **2002**, *124*, 1658−1663. (d) Gohy, J.-F.; Lohmeijer, B. G. G.; Varshney, S. K.; Decamps, B.; Leroy, E.; Boileau, S.; Schubert, U. S. *Macromolecules* **2002**, *35*, 9748−9755.
(10) (a) Zhu, J.; Munn, R. J.; Nantz, M. H. *J. Am. Chem. Soc.* **2000**, *122*, 2645−2646. (b) Guo, X.; Szoka, F. C. *Acc. Chem. Res.* **2003**, *36*, 335−341. (c) Johnsson, M.; Wagenaar, A.; Engberts, J. B. F. N. *J. Am. Chem. Soc.* **2003**, *125*, 757−760. (d) Chécot, F.; Lecommandoux, S.; Gnanou, Y.; Klok, H.-A. *Angew. Chem., Int. Ed.* **2002**, *41*, 1339−1343. (e) Lee, M.; Lee, S.-J.; Jiang, L.-H. *J. Am. Chem. Soc.* **2004**, *126*, 12724−12725.
(11) (a) Ryu, J.-H.; Kim, H.-J.; Huang, Z.; Lee, E.; Lee, M. *Angew. Chem., Int. Ed.* **2006**, *45*, 5304−5307. (b) Ajayaghosh, A.; Chithra, P.; Varghese, R. *Angew. Chem., Int. Ed.* **2007**, *46*, 230−233.
(12) (a) Kim, B.-S.; Yang, W.-Y.; Ryu, J.-H.; Yoo, Y.-S.; Lee, M. *Chem. Commun.* **2005**, 2035−2037. (b) Kim, B.-S.; Hong, D.-J.; Bae, J.; Lee, M. *J. Am. Chem. Soc.* **2005**, *127*, 16333−16337.
(13) Jang, C.-J.; Ryu, J.-H.; Lee, J.-D.; Sohn, D.; Lee, M. *Chem. Mater.* **2004**, *16*, 4226−4231.

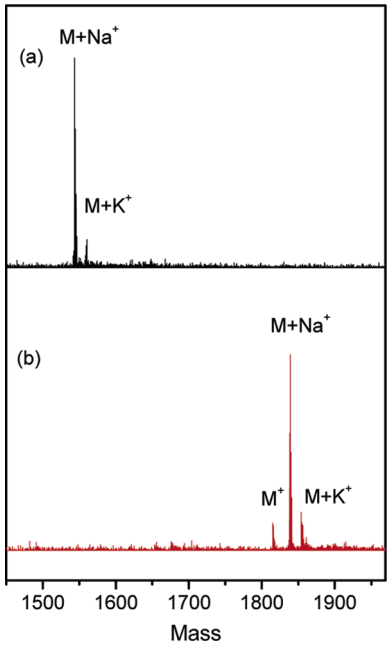

Figure 1. MALDI-TOF mass spectra of (a) **7** and (b) **8**.

and X-ray scatterings. The X-ray diffraction pattern of **7** based on a methyl group as a hydrophobic tail displays three sharp reflections with the ratio of 1:$\sqrt{3}$:2 in the low angle region that correspond to a 2D hexagonal columnar structure with a lattice constant of 4.2 nm (Figure 2a). Considering the lattice constant and extended molecular length (2.7 nm by Corey−Pauling−Koltun (CPK) molecular model), this dimension implies that the rodlike rigid segments arrange axially with their preferred direction within a cross-sectional slice of the column, in which rigid aromatic building blocks pack in an interdigitated fashion (Figure 2b).

In contrast, the X-ray diffraction pattern of **8** based on a longer hydrophobic docosyl chain displays sharp reflections that correspond to equidistant *q*-spacings and thus index to a lamellar lattice. The layer thickness obtained from the X-ray diffraction pattern appeared to be 8.3 nm, that is, much larger than the estimated molecular length (5.4 nm by CPK model), indicating that the hydrophobic parts are interdigitated (Figure 2b).[14]

The results described above demonstrate the capability of manipulating the carbohydrate-coated supramolecular structure by grafting flexible hydrophobic chains of different lengths to the apex of the same rigid building block conjugated mannose branched dendron. The variation in the supramolecular structure can be rationalized by considering the microphase separation between the dissimilar parts of the molecule and the space-filling requirement of the flexible hydrophobic chains. Molecule **7** based on a methyl group at the end of the rod segment can be packed with fully interdigitated fashion of the rod segments, and the bulky dendritic geometry of the flexible segments is likely to frustrate the 2D growth of a self-assembled structure, which results in carbohydrate-coated 1D cylinders. Increasing the length of the hydrophobic chain, however, prohibits the interdigitaion of the rod segments due to phase separation between aromatic rods and alkyl chains, resulting in the formation of carbohydrate-coated 2D sheets.

(14) The layer structure of **8** was further confirmed by TEM. See the Supporting Information.

Aggregation Behavior in Aqueous Solution. Dynamic light scattering (DLS) experiments were performed with **8** in aqueous solution to investigate the aggregation behavior.[15] The CONTIN analysis of the autocorrelation function showed a broad peak corresponding to a hydrodynamic radius (R_H) ranging from several nanometers to hundreds of nanometers (Figure 3a). The formation of cylindrical micelles was confirmed by the Kratky plot that shows a linear angular dependence over the scattering light intensity of the aggregates (Figure 3b).[16] The evidence for the formation of the cylindrical aggregates was also provided by transmission electron microscopy (TEM) experiments (Figure 3c). The micrographs negatively stained with a 2 wt % aqueous solution of uranyl acetate show discrete cylindrical objects with a uniform diameter of about 9 nm and a length of several hundred nanometers. Considering the extended molecular length (5.4 nm), the diameter of 9 nm indicates that the docosyl chains within the core are fully interdigitated with each other. On the basis of these results, it can be considered that **8** self-assembles into cylindrical micelles consisting of a hydrophobic core surrounded by hydrophilic mannose units in contact with the aqueous environment. Similar to **8**, **7** also formed cylindrical micelles with dimensions of several hundred nanometers long and a diameter of 8 nm in aqueous solution, as evidenced by DLS and TEM.[17]

Remarkably, these cylindrical objects transformed into spherical objects on addition of Nile Red above 1 mol % relative to the carbohydrate conjugate molecules.[18] As shown in Figure 4a, the relaxation time of a mixture solution of Nile Red and **8** in the correlation function is shorter than that of **8**. The CONTIN analysis of the correlation functions in DLS experiments with the solution containing the guest molecule showed R_H to be 7 nm (Figure 4b). These results indicate that the cylindrical micelles change into spherical micelles on addition of the hydrophobic guest molecule. The formation of spherical objects was further confirmed by TEM (Figure 4c). The micrographs revealed spherical objects with an average diameter of about 14 nm, which is in good agreement with the results obtained by DLS. Upon removal of the guest molecule by extraction with *n*-hexane, the original cylindrical objects were observed to be fully recovered as confirmed by DLS and TEM, thus indicating that this structural transformation is reversible depending on the presence of hydrophobic aromatic substrates (Figure 4b).

This phenomenon can be rationalized by considering the interruption of the packing of the rod segments by intercalation of guest molecules. The Nile Red would intercalate between the aromatic cores of the cylindrical micelles through hydrophobic and $\pi-\pi$ interactions. This intercalation causes the packing of the aromatic segments within the core to be loose. As a result, the cylindrical micelles might break up into spherical micelles (Figure 5). The intercalation of Nile Red in rod segments of **8** was confirmed by using fluorescence spectroscopy (Figure 4d). When the solution of **8** and Nile Red was excited at 294 nm, where most of the radiation is absorbed by **8**, the intensity corresponding to the emission of **8** significantly

(15) Gohy, J. F.; Lohmeijer, B. G. G.; Alexeev, A.; Wang, X. S.; Manners, I.; Winnik, M. A.; Schubert, U. S. *Chem.-Eur. J.* **2004**, *10*, 4315−4323.
(16) Fujita, H. *Polymer Solutions*; Elsevier Science: New York, 1990.
(17) See the Supporting Information.
(18) The transformation behavior of **7** and **8** was shown to be essentially the same. The transformation occurred by addition of a small amount of hydrophobic guest molecules such as Nile Red, nitrobenzene, and 4−4′-dinitrobiphenyl. See the Supporting Information.

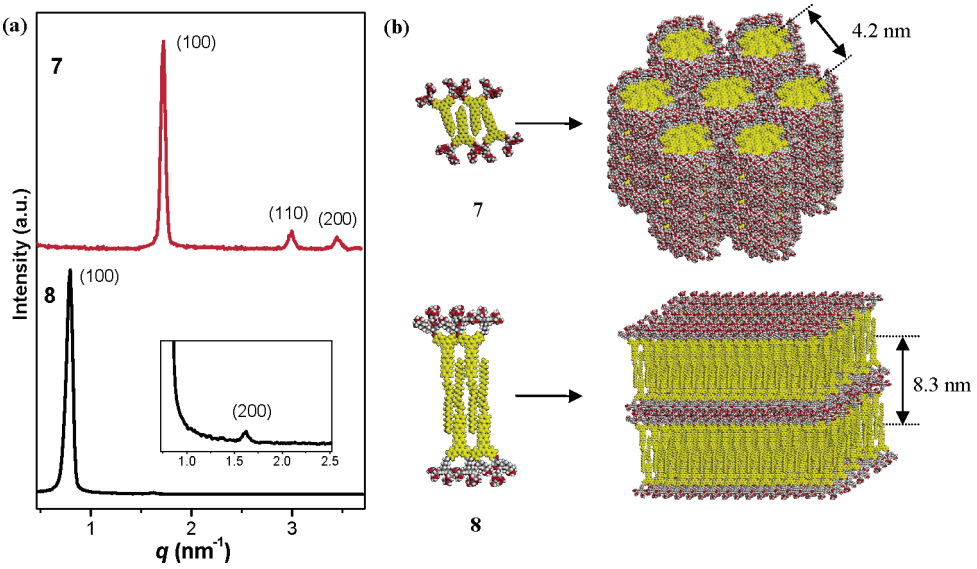

Figure 2. (a) X-ray diffraction patterns of **7** and **8** measured at 25 °C. (b) Schematic representation for the hexagonal columnar structure of **7** and the lamellar structure of **8** in the solid state.

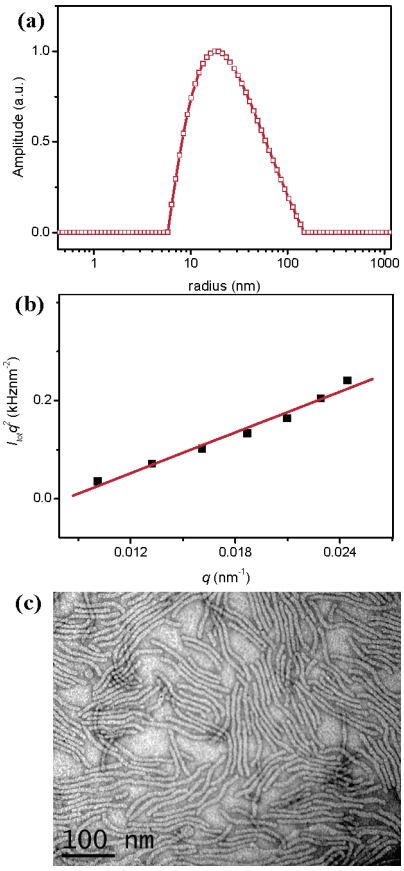

Figure 3. (a) The size distribution graph at scattering angle of 90° from CONTIN analysis of the autocorrelation function of laser light scattering of aqueous solution of **8** (0.1 wt %). (b) Kratky plot (■) and linear fit (−). (c) TEM image of **8** with negative staining.

decreases while exhibiting another emission at 620 nm corresponding to Nile Red. This result indicates that energy transfer takes place between the aromatic units of Nile Red and those of **8** within the supramolecular micelles,[19] suggesting that the insertion of Nile Red between the rod parts of **8** in cylindrical micelles seems to interfere with the compact rod packing and break up the cylinders to form the spheres.

To investigate the amount of dye encapsulation, UV/vis spectroscopic experiments were performed via addition of Nile Red in an aqueous solution of carbohydrate conjugate aromatic molecules. The absorbance at absorption maximum of Nile Red was plotted against the molar ratio of dye and each of the molecules **7** and **8**. As shown in Figure 6, the absorbance increases with an increase in the ratio up to a certain point at which the absorbance does not change with further increment of the ratio. Therefore, the maximum mol percent of dye loading per each molecule in the aqueous phase can be estimated to be approximately 5% and 30% for **7** and **8**, respectively. These results demonstrate that the micelles self-assembled by the molecule **8** can encapsulate much more guest molecules than **7** because long hydrophobic tails can provide more hydrophobic space for the guest molecules. The entrapment of a hydrophobic guest within the micelles can be rationalized by the strong hydrophobic and $\pi-\pi$ associations between the guest and the amphiphilic molecule, and the poor solubility of the guest molecule in water.

Biological Activities as a Multivalent Ligand. Self-assembly of the amphiphiles into supramolecular objects coated by carbohydrates suggests that they may function as supramolecular multivalent ligands. Toward this direction, the quantitative precipitation assay with lectin concanavalin A (Con A) was selected because Con A recognizes α-D-mannopyranoside, and these systems have been extensively studied as a model of multivalent interactions (Figure 7).[20] Multivalent interactions between mannose residues on the nanostructures and Con A that were fluorescently labeled with fluorescein resulted in the mutual cross-linking, thereby inducing the precipitation of the mixture.[21] After centrifugation, the degree of precipitation could be determined by measuring the fluorescence intensity of the soluble Con A fraction. Both cylindrical and spherical micelles showed a similar efficient precipitation capability, indicative of strong binding of mannose-coated supramolecular structures

(19) Ryu, J.-H.; Lee, M. *J. Am. Chem. Soc.* **2005**, *127*, 14170−14171.

(20) (a) Osawa, T.; Matsumoto, I. *Methods Enzymol.* **1972**, *28*, 323−327. (b) Woller, E. K.; Cloninger, M. J. *Org. Lett.* **2002**, *4*, 7−10.

(21) Strong, L. E.; Kiessling, L. L. *J. Am. Chem. Soc.* **1999**, *121*, 6193−6196.

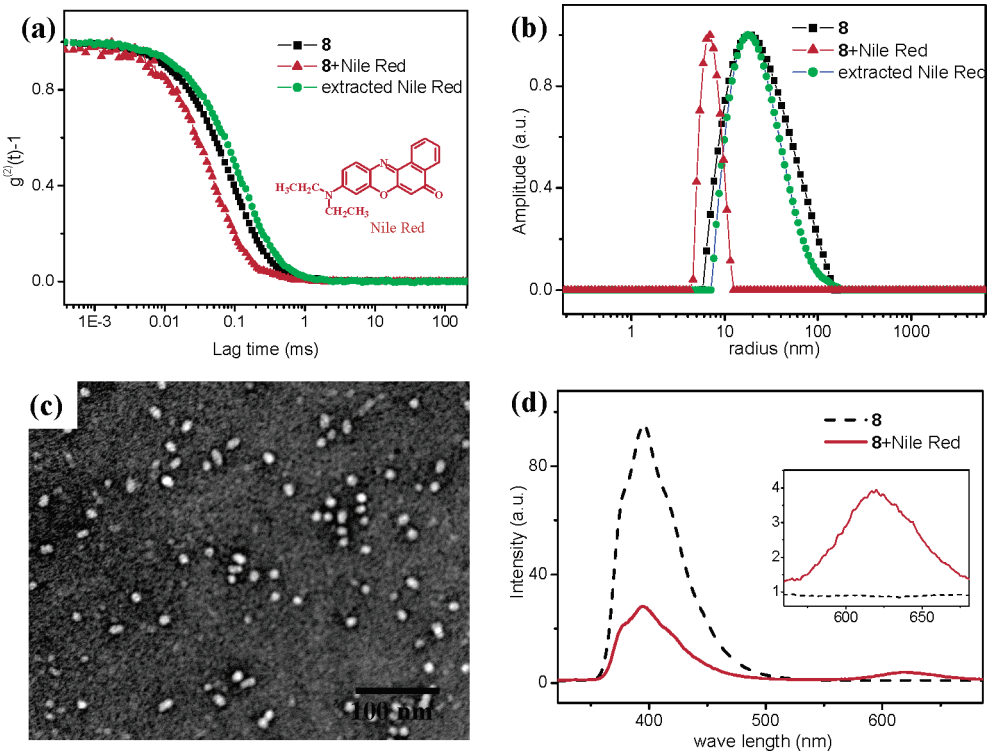

Figure 4. (a) Autocorrelation functions and (b) size distribution graph at scattering angle of 90° from CONTIN analysis of the autocorrelation function of laser light scattering of aqueous solution of **8** (0.1 wt %), mixture solution (0.1 wt %) of **8** and Nile Red (30 mol % relative to **8**), and solution after extraction of Nile Red. (c) TEM image for the spherical micelles (**8**·Nile Red) with negative staining. (d) Emission spectra of the aqueous solution of **8** and of **8**·Nile Red aqueous solution (0.1 wt % Nile Red; 30 mol % relative to **8**; excitation wavelength 294 nm; inset: magnification between 550 and 700 nm).

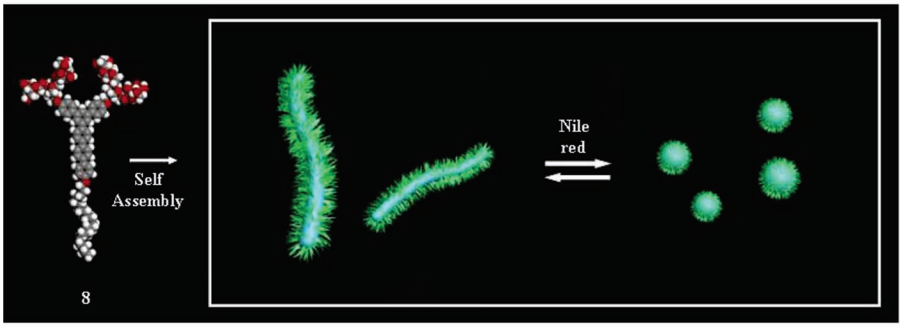

Figure 5. The schematic representation of the reversible transformation of cylindrical micelles into spherical micelles.

to Con A. It should be noted that the precipitation was reversible when a high excess of methyl mannoside (1000×) was added to the precipitates. In contrast, a galactose, nonspecific to Con A, was not able to reverse the precipitation, indicating that the interaction is specific to mannose units.

Interestingly, both cylindrical and spherical micelles appeared to specifically bind to the multiple mannose binding proteins (MBPs) of bacterial pili in *Escherichia coli* (ORN 178), demonstrating that the mannose-coated objects are excellent multivalent ligands toward the specific receptors on the cell surface.[22] As shown in Figure 8, a number of cylindrical and spherical objects were clearly observed to be located along the fibers, indicative of strong binding of the objects to the MBPs. Notably, the shape and size of the objects were retained even after binding to the bacterial pili, indicative of high stability of the supramolecular objects. The strong binding between the objects and the MBPs seems to be attributed to recognition of multivalent α-D-mannopyranoside ligands on the surface of a micellar object by the receptors located on the bacterial pili. This binding event was observed to be specific to the α-D-mannopyranoside-coated objects. To confirm the selective binding to MBPs, ORN 208 *E. coli* cells lacking the MBPs were incubated with the nano-objects. In contrast to the ORN 178 strain, no supramolecular objects appeared to be imaged through TEM, indicating that the bacterial pili of the ORN 208 strain are unable to mediate α-D-mannopyranoside selective binding. These results demonstrate that carbohydrate-coated objects designed as multivalent nanoscaffolds for use in selective receptor binding can be constructed from self-assembly of carbohydrate conjugate aromatic amphiphiles.

In addition, the spherical micelles (**8**·Nile Red) can be used as scaffolds for the selective labeling of a specific cell as the micelles contain fluorescent dye. To investigate the potential application as a cell labeling system, the spherical micelles (**8**·Nile Red) were added to the ORN 178 *E. coli* solution, and the mixture was observed using a fluorescence microscope. As

(22) Harris, S. L.; Spears, P. A.; Havell, E. A.; Hamrick, T. S.; Horton, J. R.; Orndorff, P. E. *J. Bacteriol.* **2001**, *183*, 4099−4102.

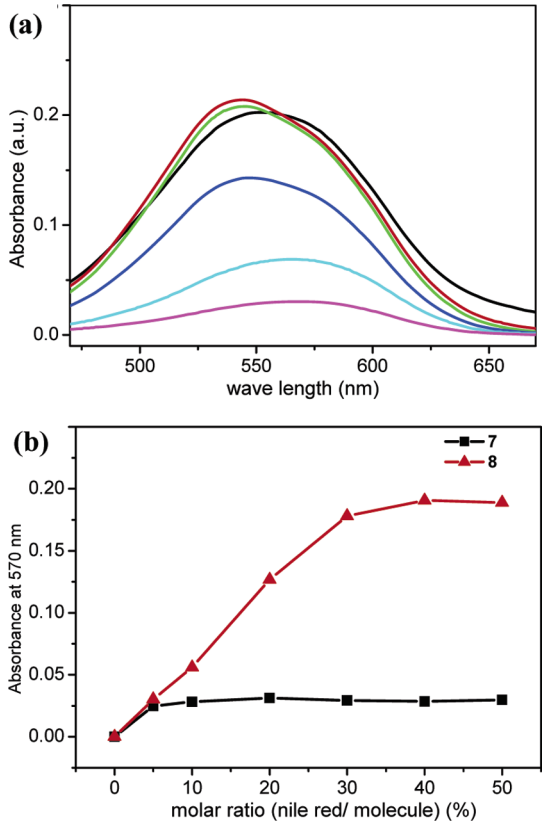

Figure 6. (a) UV−vis spectrum for Nile Red dye encapsulated within **8** solution in water at various ratios of Nile Red/**8** (mol/mol) (a range of ratio from 0.05 to 1 mol/mol). (b) Absorbance intensity of Nile Red at 550 nm as a function of the ratio of Nile Red/molecules (mol/mol).

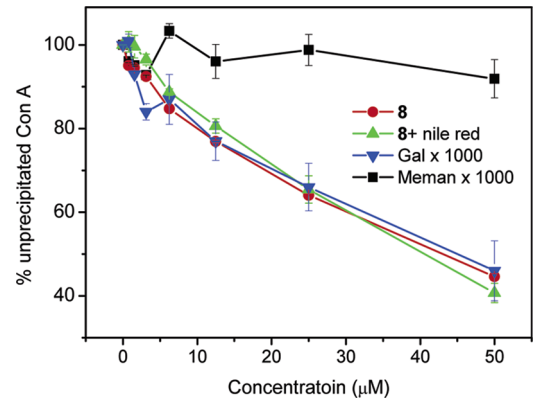

Figure 7. (a) The quantitative precipitation assay with lectin concanavalin A. Each value represents the mean ± s.d. (n = 3).

shown in Figure 9a, ORN 178 *E. coli* could be easily detected with red fluorescence of Nile Red, whereas no red fluorescence was detected with cylindrical micelle (**8**) and when ORN 208 *E. coli*, which does not contain mannose-specific protein, was treated with the dye containing spherical micelles. These results imply that the carbohydrate-coated nanostructure with entrapped dye molecules can have potential applications from target selective nanocarriers, to labeling of specific protein on the cell surface, to sensing of a range of pathogens.

To investigate the effect of the shape of nanostructure as multivalent ligands, nanofibers (**8**) and spherical micelles (**8**·Nile Red) were added to the ORN 178 *E. coli* solution, respectively. Upon the addition of carbohydrate-coated objects, we found on the optical microscope that both cylindrical and

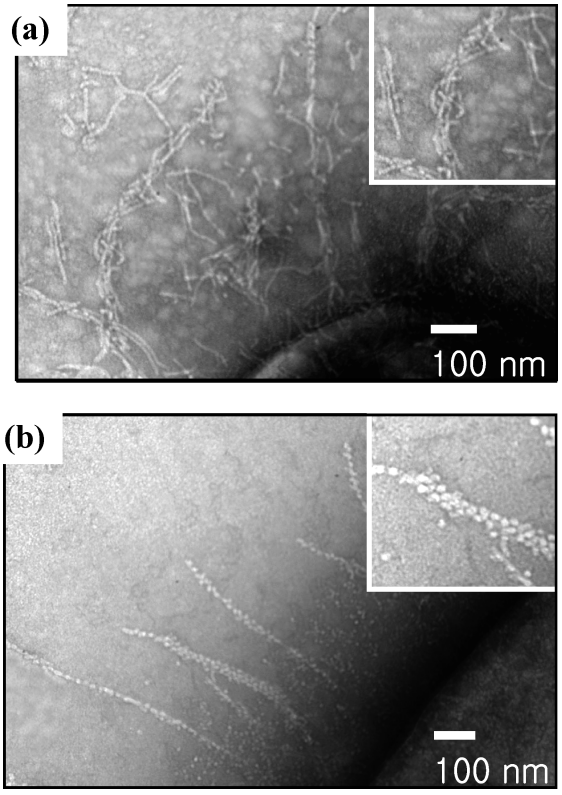

Figure 8. TEM images with negative staining of a sectioned area of pili of the *E. coli* ORN 178 strain bound with (b) cylindrical (**8**) and (c) spherical micelles (**8**·Nile Red). A portion of an *E. coli* is shown in the lower right.

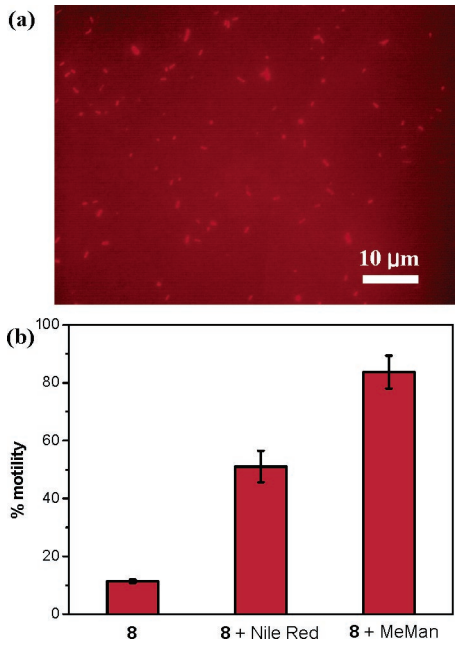

Figure 9. Fluorescence microscope image of the *E. coli* ORN 178 strain bound with spherical micelles (**8**·Nile Red). (b) Bacterial motility inhibition assay. Each value represents the mean ± s.d. (n = 3).

spherical micelles could inhibit motility of the *E. coli* ORN178 strain (Figure 9b).[6b] The motility inhibition occurred immediately after addition of micellar solution into *E. coli* solutions. However, the degree of *E. coli* motility inhibition with the spherical micelles (**8**·Nile Red) was observed to be significantly lower than that with the nanofibers (**8**). It seems that multivalent interactions between the mannoses on the

nanostructures and the MBPs cause intra-bacterial pili aggregation and that aggregation might interfere with flagella motion followed by the inhibition of bacterial motility. Again, the inhibition was observed to be reversible by the addition of methyl mannoside in high excess, but not by nonspecific galactose. Other evidence of specificity is that all of the nanostructures were not able to inhibit motility of a bacterial strain that lacks the MBPs (ORN208).

The results from the experiments described above, Con A precipitation and the inhibition of *E. coli* motility, imply that there are size dependencies on the outcome of the interaction. Con A tetramer has dimensions of 6.7 × 11.3 × 12.2 nm,[23] whereas *E. coli* cells are more than 100× larger than Con A. We explain the difference in the outcome of the interaction as the Con A being unable to distinguish the size between the short (spherical) and long (cylindrical) nanostructures, as the size of spherical micelle from **8**• Nile Red is already similar to that of Con A tetramer. In contrast, as also can be evidenced from TEM observation, a comparatively large *E. coli* cell should feel the nanostructures differently. The spherical micelles are too short to cross-link the pili, whereas long cylinders are able to cross-link the pili. As a result, the degree of motility inhibition of *E. coli* can be manipulated by controlling the shape of the nanostructure.

Conclusions

New carbohydrate conjugate aromatic amphiphiles were synthesized, and their self-assembling behavior in both bulk and aqueous solution was investigated. In the bulk state, the carbohydrate conjugate molecule based on a short hydrophobic tail was observed to self-assemble into a carbohydrate-coated columnar structure, whereas the molecule based on a long hydrophobic tail self-assembled into a carbohydrate-coated sheet structure. In aqueous solution, both amphiphiles self-assemble into well-defined discrete carbohydrate-coated nanofibers with a uniform diameter. Interestingly, these nanofibers reversibly transform into a spherical micellar structure on addition of guest molecules. Both objects functioned as supramolecular multivalent ligands for lectin, Con A, and the receptors on *E. coli*. In particular, the spherical objects were shown to be applicable for labeling specific protein on cell surface due to entrapment of fluorescent dye molecules. In addition, motility inhibition experiments showed that the shape of supramolecular architecture has a significant effect on the biological activity. These results demonstrate that the ability of supramolecular cylinders to be in response to external stimuli can provide novel opportunities to control many biological activities.

Acknowledgment. This work was supported by the Creative Research Initiative Program of the Korean Ministry of Science and Technology and Pohang Accelerator Laboratory, Korea. E.L. thanks the Seoul Science Fellowship Program.

Supporting Information Available: Experimental details. This material is available free of charge via the Internet at http://pubs.acs.org.

JA070173P

(23) Bouckaert, J.; Poortmans, F.; Wyns, L.; Loris, R. *J. Biol. Chem.* **1996**, *271*, 16144−16150.

Supporting Information

Carbohydrate-Coated Supramolecular Structures: Transformation of Nanofibers into Spherical Micelles Triggered by Guest Encapsulation

Ja-Hyoung Ryu, Eunji Lee, Yong-beom Lim, and Myongsoo Lee*

Center for Supramolecular Nano-Assembly and Department of Chemistry, Yonsei University, Seoul 120-749, Korea

E-mail: mslee@yonsei.ac.kr

Experimental section

Materials

NaH (60%), *p*-toluene-sulfonyl chloride (98%) from Tokyo Kasei were used as received. D(+)-Mannose (99%), *tert*-butyldimethylsilyl chloride (97%), tetrabutyl-ammonium fluoride (1.0 M solution in tetrahydrofuran), benzyl bromide (98%), sodium methoxide (95%), iodomethane (99%), 1-bromododecane (97%), palladium on carbon 5 wt%, ethylene glycol (95%), *n*-butyl lithium (1.6M solution in *n*-hexane), borane-THF complex (1.0M solution in THF), tetrakis (triphenylphosphine) palladium (0) (99%), triisopropyl borate (98+%), iodine monochloride (1.0M solution in dichloromethane), 3-chloro-2-chloromethyl-1-propene (99%) (all from Aldrich) and the conventional reagents were used as received. Unless otherwise indicated, all starting materials were obtained from commercial suppliers (Aldrich, Lancaster, TCI, etc.). All atmosphere sensitive reactions were done under nitrogen. Flash column chromatography was carried

out with Silica Gel 60 (230-400 mesh) from EM Science. Bromo-2,3,4,6-tetra-*O*-acetyl-α-D-mannopyranoside was prepared according to the procedures described previously.[1] For synthetic detail, see the Supporting Information. ^{1}H and ^{13}C NMR spectra were recorded from $CDCl_3$ or DMSO solutions on a Bruker AM 250 spectrometer. The purity of the products was checked by thin-layer chromatography (TLC; Merck, silica gel 60). Microanalysis was performed with a Perkin Elmer 240 elemental analyzer. Dynamic light scattering measurements were performed using a UNIPHASE He-Ne laser operating at 632.8 nm. The maximum operating power of the laser was 30 mW. The detector optics employed optical fibers coupled to an ALV/SO-SIPD/DUAL detection unit, which employed an EMI PM-28B power supply and ALV/PM-PD preamplifier/discriminator. The signal analyzer was an ALV-5000/E/WIN multiple tau digital correlator with 288 exponentially spaced channels. MALDI-TOF mass was performed on a Perseptive Biosystems Voyager-DE STR using a 2,5-dihydroxy benzoic acid matrix. X-ray scattering measurements were performed in transmission mode with synchrotron radiation at the 3C2 X-ray beam line at Pohang Accelerator Laboratory, Korea. For TEM measurements, 3 μL of an aqueous solution of sample was placed onto a holey carbon-coated copper grid, and 3 μL of 2 % (w/w) uranyl acetate solution was added for negative stain. The sample was deposited for 1 min, and excess solution was wicked off by filter paper. The dried specimen was observed with a JEOL-JEM 2010 instrument operating at 120 kV. The data were analyzed with Digital Micrograph software. In case of solid sample, the sample was microtomed at room temperature using a cyro-ultramicrotome without staining. Optical absorption spectra were obtained from a Shimadzu 1601 UV spectrophotometer. The steady-state fluorescence spectra were obtained from a Hitachi F-4500 fluorescence spectrophotometer.

Quantitative Con A precipitation: Fluorescein labeled Con A was obtained from Vector laboratories. The Con A was diluted into a concentration of 0.5 mg/mL with 10 mM Hepes, 0.15 M NaCl, 0.1 mM Ca^{2+}, 0.01 mM Mn^{2+}, 0.08% NaN_3, pH 7.5. Twenty microliters of the Con A solution was mixed with an equal volume of the object solution in water. The mixture incubated for 10 min at room temperature, centrifuged for 3 min, and 20 μL of supernatant was taken. The fluorescence from non-precipitated Con A was measured at 495 nm (excitation) and 516 nm (emission).

***E. coli* motility inhibition assay**: Overnight culture of *E. coli* strain ORN178 was diluted into the concentration of 5×10^7 cells/mL with phosphate buffered saline (PBS). Two microliters of the *E. coli* solution was placed onto glass slide and 2 μL of serially diluted solutions of the objects in water were added. The sample was covered with a cover glass and a layer of rubber cement was placed around the edges. The *E. coli* was observed with Nikon Eclipse TE2000-U inverted fluorescence microscope equipped with DXM1200C digital camera. For the motility inhibition assay, time-lapse images were analyzed using Adobe Premiere software. The % motility was expressed as (number of mobile cells / number of total cells) ×100.

UV-Vis spectroscope: To investigate the amount of dye encapsulation, the prepared Nile Red solution (1×10^{-3} M in methylene chloride) was added to aqueous solutions (1.0×10^{-4} M) of the carbohydrate conjugate aromatic molecules with different mole ratios, [Nile Red] / [molecule], from 0.05 to 1 and sonicated for a few hours at room temperature to allow for reaching equilibrium. The methylene chloride was removed via evaporation. After being filtered through 0.45 μm hydrophilic filter (0.45 μm pore PVDF membrane filter), UV/vis spectroscopy measurements were performed with the variation in Nile Red content at the fixed solution of molecule in

water (1.0 x 10^{-4} M).

Synthesis. The synthetic procedures used in the preparation of mannose-branched amphiphilic molecules is described in Scheme 1.

Synthesis of *tert*-butyldimetylsilyloxyethyl 2,3,4,6-tetra-*O*-acetyl-α-D-mannopyranoside (1).

To a solution of bromo 2,3,4,6-tetra-*O*-acetyl-mannopyranoside (25 g 63.7 mmol) in acetonitrile solution (200 mL) was added derierite (10 g), excess ethylene glycol (20 g, 322 mmol) and mercury(II) cyanide (24.0 g, 101 mmol). The mixture was stirred for overnight at room temperature and then filtered. The resulting residue was dissolved chloroform (200 mL) and washed with $NaCl_{(sat)}$. The organic layer was dried over anhydrous magnesium sulfate and filtered and concentrated. The crude product was purified by a flash column chromatography (silica gel, EtOAc: hexane = 1: 1) to yield 12.3 g (60%). ^{1}H-NMR (250 MHz, $CDCl_3$, ppm): δ = 5.22-5.12 (m, 3H; H-2, H-3, H-4), 4.78 (d, *J*=1.5 Hz, 1H; H-1), 4.18 (dd, *J*=12.0, 5.5 Hz, 1H; H-6a), 4.03-3.95 (m, 3H; H-6b, H-5), 3.68-3.53 (m, 4H; OCH_2CH_2OH), 2.05 2.00 1.94 1.91 (s, 12H; H_3CC=O).

The above compound (12.3 g, 31.3 mmol) was dissolved in CH_2Cl_2 (100 mL) and added *tert*-butyldimethylsilyl chloride (TBDMSCl) (7 g, 46.4 mmol) and imidazol (4.2 g, 61.5 mmol). The mixture was stirred for 2 hours at room temperature. Then the resulting solution was washed with 1M $NaHCO_3$ solution and the methylene chloride solution was dried over anhydrous magnesium sulfate, and filtered. The solvent was removed in a rotary evaporator, and the crude product was purified by a flash column chromatography (silica gel, EtOAc: hexane = 1: 1) to yield 14.8 g (93%). ^{1}H-NMR (250

MHz, $CDCl_3$, ppm): δ = 5.22-5.12 (m, 3H; H-2, H-3, H-4), 4.78 (d, *J*=1.5 Hz, 1H; H-1), 4.18 (dd, *J*=12.0, 5.5 Hz, 1H; H-6a), 4.03-3.95 (m, 3H; H-6b, H-5), 3.68-3.53 (m, 4H; O*CH*$_2$*CH*$_2$OSi), 2.05 2.00 1.94 1.91 (s, 12H; *H*$_3$CC=O), 0.89(m, 12H; Si(CH_2)$_2$(C*(CH*$_3$*)*$_3$)), 0.08 (m, 6H; SiC*(CH*$_3$*)*$_2$(C(CH_3)$_3$)).

Synthesis of hydroxyethyl 2,3,4,6-tetra-*O*-benzyl-α-D-mannopyranoside (2).

Sodium methoxide (50 mg, 2.1 mmol) was added to a solution of **1** (14.8 g, 29.2 mmol) in methanol (100 mL). After the mixture had been stirred for 4 h at room temperature, was treated with ion-exchange regin and filtered and concentrated to yield hydroxyethyl-α-D-mannopyranoside (9.1 g, in 92% yield). ^{1}H-NMR (250 MHz, $CDCl_3$, ppm): δ 4.86 (d, *J*=1.5 Hz, 1H; H-1), 3.97-3.49 (m, 10H; H-2, H-3, H-4, H-5, H-6, O*CH*$_2$*CH*$_2$OSi), 0.89 (m, 12H; Si(CH_2)$_2$(C*(CH*$_3$*)*$_3$)), 0.08 (m, 6H; SiC*(CH*$_3$*)*$_2$(C(CH_3)$_3$)).

The solution of NaH (8.4 g, 350 mmol) in DMF (100 mL) was dropped the solution of the above compound (9.1 g, 26.9 mmol) in DMF (50 mL) in ice bath. Then benzyl bromide (41.46 mL, 350 mmol) was dropped slowly and stirred for 24 h at room temperature. The solution was quenched with MeOH and DMF was removed by vacuum distillation. The residue was extracted with methylene chloride and dried over anhydrous magnesium sulfate, and filtered and concentrated. The crude product was dissolved dried THF (100 mL) and added with 1M TBAF solution (34.3 mL). The mixture solution was stirred for 2 h at room temperature and the solvent was removed in a rotary evaporator, and the crude product by flash column chromatography (silica gel, ethyl acetate/hexane = 4:1) to yield 6.3 g (40.1%). ^{1}H-NMR (250 MHz, $CDCl_3$, ppm): δ 7.37-7.14 (m, 20Ar-H; OCH$_2$*phenyl*), 4.91 (d, *J*=1.5 Hz, 1H; H-1), 4.85-4.48 (m, 8H; O*CH*$_2$phenyl), 3.91-3.67 (m, 10H; H-2, H-3, H-4, H-5, H-6, O*CH*$_2$*CH*$_2$OH).

Synthesis of Compound 3.

Dry NaH (0.52 g, 21.7 mmol), 3-chloro-2-chloromethyl-1-propene (0.68 g, 5.5 mmol), and freshly distilled dry THF (50 mL) were placed in a dry round bottomed flask under N_2 gas. The compound **2** (6.3 g, 10.8 mmol) was added dropwise to this mixture at room temperature, and the mixture was stirred at 65 ^{o}C for 12 h. After cooling to room temperature, the reaction mixture was quenched with water and extracted with diethyl ether. The organic layer was dried over anhydrous $MgSO_4$, the solvent was removed in a rotary evaporator, and the crude product was purified by column chromatography (silica gel) with ethyl acetate and hexane (2:1 v/v) as eluent to give a colorless liquid (6.6 g, in 96% yield). ^{1}H-NMR (250 MHz, $CDCl_3$, ppm): δ 7.37-7.14 (m, 40Ar-H; OCH_2*phenyl*), 5.13 (s, 2H; *CH_2*C), 4.91 (d, *J*=1.5 Hz, 2H; H-1), 4.85-4.48 (m, 16H; O*CH_2*phenyl), 3.98-3.50 (m, 24 H; H-2, H-3, H-4, H-5, H-6, O*CH_2CH_2*OCH_2, CH_2C*CH_2*O).

Freshly distilled dry THF (5 mL) and the above compound (6.6 g, 5.4 mmol) were placed in a dry round bottomed flask under N_2 and cooled to 0 ^{o}C in ice bath. A solution of BH_3 (1 M) in THF (11 mL) was added slowly to this mixture, which was then stirred at 0 ^{o}C for 2 h. The reaction mixture was quenched with a solution of NaOH in water (2 M, 4 mL) and allowed to stir for 15 min. This was followed by addition of an H_2O_2 aqueous solution of (30%, 4 mL), and the mixture was stirred at room temperature for 30 min. The reaction mixture was saturated with K_2CO_3 and extracted with diethyl ether. The organic layer was dried over anhydrous $MgSO_4$, the solvent was removed in a rotary evaporator, and the crude product was purified by column chromatography (silica gel) with ethyl acetate and hexane (2:1 v/v) as eluent to afford a

colorless liquid (6.5 g, in 97% yield). ^{1}H-NMR (250 MHz, $CDCl_3$, ppm): δ 7.37-7.14 (m, 40Ar-H; OCH_2*phenyl*), 4.91 (d, *J*=1.5 Hz, 2H; H-1), 4.88-4.50 (m, 16H; O*CH*$_2$phenyl), 3.98-3.50 (m, 26H; H-2, H-3, H-4, H-5, H-6, O*CH*$_2$*CH*$_2$$OCH_2$, CH*CH*$_2$$OCH_2$ and CH*CH*$_2$OH), 2.04 (m, 1H; CH_2*CH*$(OCH_2)_2$).

The above compound (6.5g, 5.2 mmol) were dissolved of dry dichloromethane (80 mL), pyridine (10 mL), and TsCl (1.5 g, 7.8 mmol) was then added under nitrogen. The reaction mixture was stirred at 25^{o}C under nitrogen for 12 h. The resulting solution was washed with water, and the dichloromethane solution was dried over anhydrous magnesium sulfate and filtered. The solvent was removed in a rotary evaporator, and the crude product was purified by column chromatography (silica gel) with ethyl acetate and hexane (2:1 v/v) as eluent to give a colorless liquid (5.5 g, in 75% yield). ^{1}H-NMR (250 MHz, $CDCl_3$, ppm): δ 7.79 (d, *J*=4.0 Hz, 2Ar-H; *o* to SO_3), 7.37-7.14 (m, 42Ar-H; OCH_2*phenyl*, *m* to SO_3), 4.91 (d, *J*=1.5 Hz, 2H; H-1), 4.88-4.50 (m, 16H; O*CH*$_2$phenyl), 3.98-3.50 (m, 26H; H-2, H-3, H-4, H-5, H-6, O*CH*$_2$*CH*$_2$$OCH_2$, CH*CH*$_2$$OCH_2$, SO_3*CH*$_2$CH), 2.44 (s, 3H; SO_3phenyl*CH*$_3$), 2.24 (m, 1H; CH_2*CH*$(CH_2O)_2$).

Synthesis of Compound 4.

Compound **4** was synthesized using a similar procedure described previously.[2] ^{1}H-NMR (250 MHz, DMSO, ppm): δ = 9.59 (s, 2H; Ar-*OH*), 7.79-7.65 (m, 13Ar-H), 7.55(d, *J*=8.5 Hz, 2Ar-H; *o* to I), 6.87 (d, *J*=8.6 Hz, 4Ar-H; *o* to OH).

Synthesis of Compound 5.

Compound **4** (0.5 g, 0.93 mmol), compound **3** (2.7 g, 1.9 mmol) and excess K_2CO_3 were dissolved in 100 ml of anhydrous acetonitrile. The mixture was heated at

reflux for 48 h. The resulting solution was poured into water and extracted with methylene chloride. The methylene chloride solution was washed with water, dried over anhydrous magnesium sulfate, and filtered. The solvent was removed in a rotary evaporator, and the crude product was purified by column chromatography (silica gel) using ethyl acetate and hexane (1:1 v/v) as eluent to yield 2.6 g (94%) of a colorless liquid. ^{1}H-NMR (250 MHz, $CDCl_3$, ppm): δ 7.79-7.51 (m, 15Ar-H), 7.37-7.14 (m, 80Ar-H; OCH_2*phenyl*), 7.01 (d, *J*=8.6 Hz, 4Ar-H; *o* to OCH_2CH), 4.95 (d, *J*=1.5 Hz, 4H; H-1), 4.88-4.50 (m, 32H; OCH_2phenyl), 4.00-3.50 (m, 52H; H-2, H-3, H-4, H-5, H-6, $OCH_2CH_2OCH_2$, $CH_2CH(CH_2)_2O$, phenylOCH_2CH), 2.42 (m, 2H; $CH_2CH(CH_2)_2O$).

Synthesis of Compound 6.

Compound **5** (2.6 g, 0.87 mmol) and 4-hydroxy-phenyl-boronic acid (0.44 g, 1.7 mmol) were dissolved in degassed THF (70 mL). Degassed 2M aqueous Na_2CO_3 solution (70 mL) was added to the solution and then tetrakis-(triphenylphosphine)palladium(0) (5 mg, 0.5 mol%) was added. The mixture was heated at reflux for 48h with vigorous stirring under nitrogen. Cooled to room temperature, the layers were separated, and the aqueous layer was then washed twice with methylene chloride. The combined organic layer was dried over anhydrous magnesium sulfate and filtered, and concentrated. The crude product was dissolved dried THF (100 mL) and added with 1M TBAF solution (1 mL). The mixture solution was stirred for 2 h at room temperature and the solvent was removed in a rotary evaporator, and the crude product was purified by column chromatography (silica gel) using ethyl acetate and hexane (1:1 v/v) to yield 2.1 g (79.6%) of a colorless liquid. ^{1}H-NMR (250 MHz, $CDCl_3$, ppm): δ 7.79-7.51 (m, 17Ar-H), 7.37-7.14 (m, 80Ar-H; OCH_2*phenyl*), 7.01 (d, *J*=8.6 Hz, 4Ar-H;

o to OCH_2CH), 6.96 (d, *J*=8.5 Hz, 2Ar-H; *o* to OH), 4.95 (d, *J*=1.5 Hz, 4H; H-1), 4.88-4.50 (m, 32H; O*CH*$_2$phenyl), 4.00-3.50 (m, 52H; H-2, H-3, H-4, H-5, H-6, O*CH*$_2$*CH*$_2$$OCH_2$, CH_2CH(*CH*$_2$)$_2$O, phenylO*CH*$_2$CH), 2.42 (m, 2H; CH_2*CH*(CH_2)$_2$O).

Synthesis of Compounds 7 and 8.

Compounds were synthesized using the same procedure. A representative example is described for **8**. Compound **6** (0.9 g, 0.30 mmol), bromodocosane (1.16 g, 3.0 mmol) and excess K_2CO_3 were dissolved in 100 mL of anhydrous acetonitrile. The mixture was heated at reflux for 24 h. The resulting solution was poured into water and extracted with methylene chloride. The methylene chloride solution was washed with water, dried over anhydrous magnesium sulfate, and filtered, and concentrated. The solvent was removed in a rotary evaporator, and the crude product was purified by column chromatography (silica gel) using ethyl acetate and hexane (1:1 v/v) as eluent to yield 0.67 g (68%) of a waxy solid.

The above compound (0.5g, 0.15 mmol) was dissolved in methanol (20 mL) and added 5 wt% Pd-C (50 mg). The reaction mixture was stirred at r.t. under hydrogen atmosphere for 24 h until the disappearance of the starting material (TLC). The mixture was filtered through a pad of Celite, and concentrated to yield 0.27 g (96%)of a white solid.

7: mp >250 ^oC; ^{1}H-NMR (250 MHz, DMSO, ppm): δ 7.95 (d, *J*=3.8 Hz, 2Ar-H), 7.83-7.78 (m, 11Ar-H), 7.73 (d, *J*=5.5 Hz, 2Ar-H; *m* to OCH_2CH), 7.65 (d, *J*=4.0 Hz, 2Ar-H; *m* to OCH_2CH_2), 7.08 (d, *J*=4.0 Hz, 2Ar-H; *o* to OCH_2CH), 7.02 (d, *J*=4.1 Hz, 2Ar-H; *o* to OCH_2CH_2), 4.72 (d, *J*=1.5 Hz, 4H; H-1), 4.68, 4.65, 4.53, 4.42 (d, 20H; H-2, H-3, H-4, H-5) 4.05-3.98 (m, 4H; phenylO*CH*$_2$CH) 3.80 (s, 1H; phenylO*CH*$_3$), 3.66-3.45(m,

48H; H-6, O*CH*$_2$*CH*$_2$OCH$_2$, CH$_2$CH(*CH*$_2$)$_2$O,), 2.30 (m, 2H; CH$_2$*CH*(CH$_2$)$_2$O). ^{13}C-NMR (250 MHz, DMSO, ppm) : δ 159.4, 142.2, 140.2, 139.9, 138.7 133.5, 132.8, 129.2 128.6, 128.0, 127.6, 124.0, 115.9, 100.8, 74.8, 71.9, 71.2, 70.6, 69.4, 68.4, 67.9, 67.0, 66.5, 62.2, 57.2, 40.0; Anal. Calcd for :$C_{98}H_{142}O_{31}$: C, 60.78; H, 6.62. Found C, 60.49; H, 6.65; MALDI-TOF-MS *m/z* $(M+Na)^+$ 1543.2, $(M+K)^+$ 1559.5.

8: mp >250 ^{o}C; ^{1}H-NMR (250 MHz, DMSO, ppm): δ 7.95 (d, *J*=3.8 Hz, 2Ar-H), 7.83-7.79 (m, 11Ar-H), 7.73 (d, *J*=5.5 Hz, 2Ar-H; *m* to OCH$_2$CH), 7.65 (d, *J*=4.0 Hz, 2Ar-H; *m* to OCH$_2$CH$_2$), 7.08 (d, *J*=4.0 Hz, 2Ar-H; *o* to OCH$_2$CH), 7.02 (d, *J*=4.1 Hz, 2Ar-H; *o* to OCH$_2$CH$_2$), 4.72 (d, *J*=1.5 Hz, 4H; H-1), 4.68, 4.65, 4.53, 4.42 (d, 20H; H-2, H-3, H-4, H-5) 4.05-3.98 (m, 6H; phenylO*CH*$_2$CH, phenylO*CH*$_2$CH$_2$), 3.65-3.45(m, 48H; H-6, O*CH*$_2$*CH*$_2$OCH$_2$, CH$_2$CH(*CH*$_2$)$_2$O,), 2.30 (m, 2H; CH$_2$*CH*(CH$_2$)$_2$O), 1.72 (m, 2H; -OCH$_2$C*H*$_2$CH$_2$), 1.41-1.21 (m, 38H; -CH$_2$*(CH*$_2$*)*$_{19}$CH$_3$), 0.82 (t, *J*=3.4 Hz, 3H; -CH$_2$C*H*$_3$). ^{13}C-NMR (250 MHz, DMSO, ppm) : δ 159.4, 142.2, 140.2, 139.9, 138.7 133.5, 132.8, 129.2 128.6, 128.0, 127.6, 124.0, 115.9, 100.8, 74.8, 71.9, 71.2, 70.6, 69.4, 68.4, 67.9, 67.0, 66.5, 62.2, 40.0, 32.2, 29.9, 26.4 23.0, 14.5; Anal. Calcd for :$C_{98}H_{142}O_{31}$: C, 64.81; H, 7.88. Found C, 64.86; H, 7.85 ; MALDI-TOF-MS *m/z* M^+ 1815.1, $(M+Na)^+$ 1838.1, $(M+K)^+$ 1854.0.

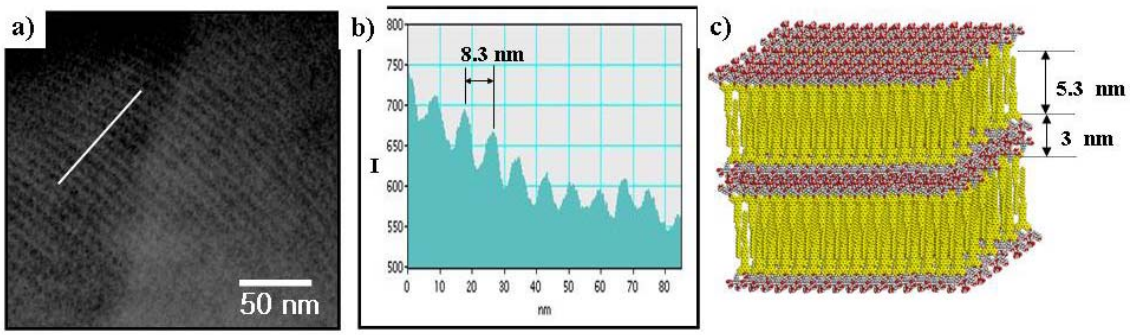

Figure S1. (a) TEM image of ultramicrotomed films of **8** stained with RuO_4 revealing layer array of alternating light hydrophilic, and dark hydrophobic layers and (b) the energy density profile. (c) Schematic representation of the layer structure. The TEM image stained with RuO_4 clearly showed a layered structure with a thickness of 8.3 nm, consistent with that obtained from X-ray diffraction pattern (Figure 2a). The layer consists of light hydrophilic part (~3 nm) and dark hydrophobic segments (~5.3 nm). Considering the molecular length of 5.4 nm and aromatic length (2 nm by Corey-Pauling-Koltun (CPK) molecular model), the dark domains with a thickness of 5.3 nm in the image suggest that the aromatic and docosyl segments are interdigitated. Considering light hydrophilic part of 3 nm in TEM image, the bulky hydrophilic segments can be considered to be packed with a bilayer fashion. Accordingly, we proposed the modified molecular packing of the layered structure.

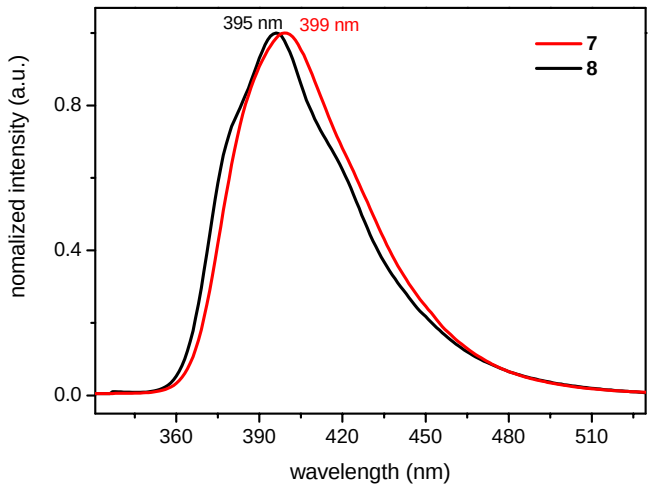

Figure S2. Emission spectra of **7** and **8** in the solid state (excitation wavelength; 300 nm). The emission maxima appear to be 395 and 399 nm for **8** and **7**, respectively and the shape of the emission curve of **7** is broader than that of **8.** These results suggest that aromatic and docosyl segments of **8** are interdigitated to an increase in the separation between aromatic segments.

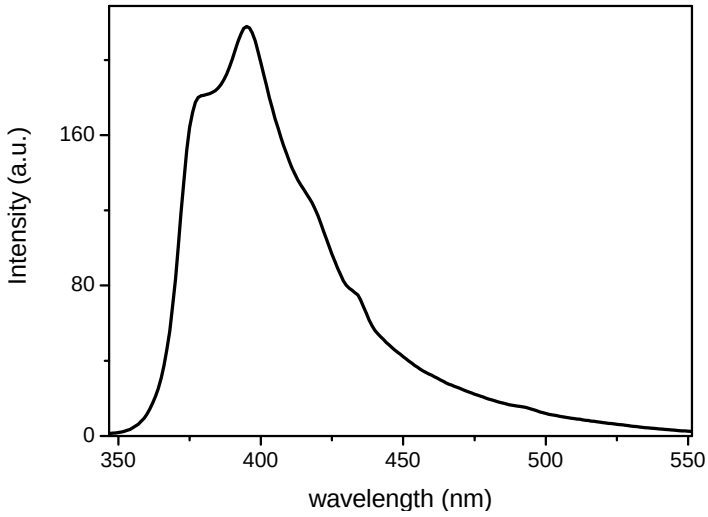

Figure S3. Encapsulation experiment. Fluorescence emission spectrum of **8** encapsulated with 10 mol percent of pyrene. The spectrum was gotten from the difference of **8** and **8** encapsulated with pyrene. Excitation wavelength was 336 nm. The ratio of the intensities of the first (371 nm) and the third (382 nm) peaks of the pyrene monomer, I_1/I_3, can be used to determine the polarity of the pyrene environment.[3] The measured I_1/I_3 ratio of 0.6 for the pyrene encapsulated in **8** indicates that the pyrene is located in the highly nonpolar microenvironment.

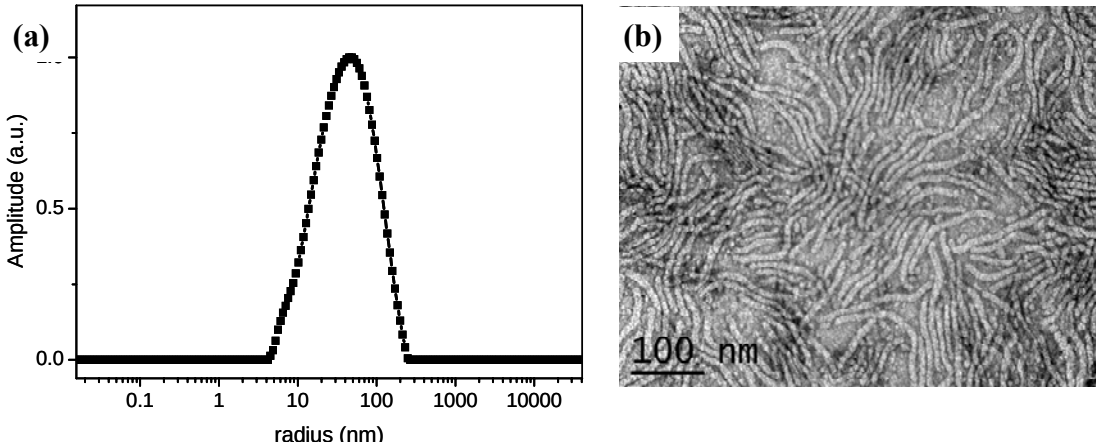

Figure S4. (a) The size distribution graph at scattering angle of 90° from CONTIN analysis of the autocorrelation function of laser light scattering of aqueous solution of **7** (0.1 wt%). (b) TEM image of **7** with negative staining.

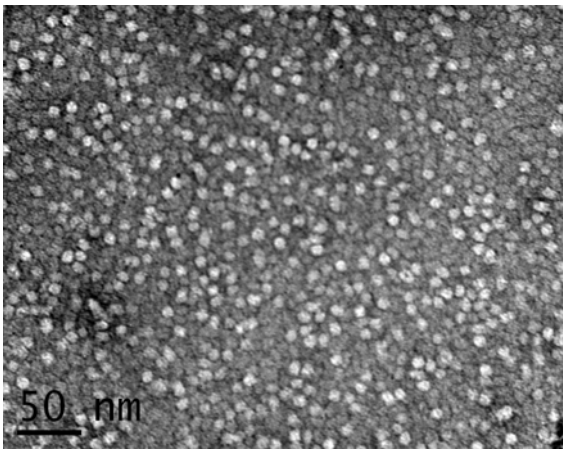

Figure S5. TEM image of mixture solution (0.01 wt%) of **7**·Nile Red (5 mol% relative to **7**) with negative staining shows the spherical shape.

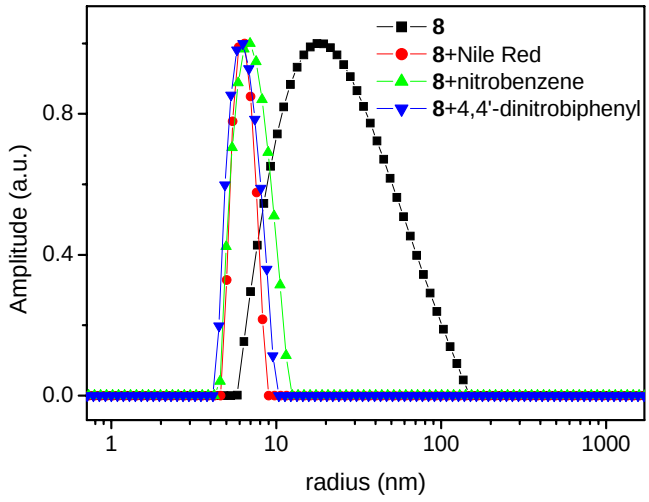

Figure S6. Size distribution graph at scattering angle of 90 ^{o} from CONTIN analysis of the autocorrelation function of laser light scattering of aqueous solution of **8** (0.1 wt%), mixture solution (0.1 wt%) of **8** and Nile Red, nitriobenzene, and 4,4'-dinitrobiphenyl.

Reference

(1) Kim, B.-S.; Yang, W.-Y.; Ryu, J.-H.; Yoo, Y.-S.; Lee, M. *Chem. Commun.* **2005**, 2035-2037.

(2) Jang, C.-J.; Ryu, J.-H.; Lee, J.-D.; Sohn, D.; Lee, M. *Chem. Mater.* **2004**, *16*, 4226-4231.

(3) (a) Kalyanasundaram, K; Thomas, J. K. *J. Am. Chem. Soc.* **1977**, *99*, 2039-2044. (b) Roxlo, C. B.; Deckman, H. W.; Abeles, B. *Phys. Rev. Lett.* **1986**, *57*, 2462-2465.